Temperature- and Frequency-Dependent Optical Constants for Nitric Acid Dihydrate from Aerosol Spectroscopy

R. F. Niedziela* and R. E. Miller

Department of Chemistry, University of North Carolina at Chapel Hill, Chapel Hill, North Carolina 27599

D. R. Worsnop

Center for Chemical and Environmental Physics, Aerodyne Research Inc., Billerica, Massachusetts

Frequency-dependent complex refractive indices have been determined from the aerosol infrared extinction spectra of laboratory-generated nitric acid dihydrate (NAD) particles. The spectra reported here were recorded at several temperatures (160, 180, and 190 K) over the mid-infrared region of the spectrum (700−4700 cm^{-1}). The optical constants retrieved from these spectra are overall in reasonable agreement with results from thin-film experiments conducted at 184 K, although there are significant differences in the intensities of several absorption bands located below 1500 cm^{-1}. We attribute these to the different methods used to make the samples in the two types of experiments and consider the substrate-free aerosol results to be unperturbed NAD. The temperature dependence of the NAD aerosol optical constants was found to be quite weak between 160 and 190 K, in contrast to the strong temperature dependence observed previously for the optical constants of water ice.

Introduction

Type I polar stratospheric clouds (PSCs) play an important role in determining the composition of the polar stratosphere. These PSCs, which are thought to be composed of nitric acid/water mixtures, provide surfaces on which heterogeneous chemical reactions can occur. This in turn perturbs the equilibrium in polar stratospheric photochemistry and results in chlorine-catalyzed ozone depletion each spring.[1−5] Sedimentation of PSC particles can also affect atmospheric chemistry by removing nitric acid from the lower stratosphere.[2,6,7] This denitrification process reduces the gas-phase concentrations of nitrogen oxide species that otherwise tend to scavenge chlorine radicals that participate in the ozone destruction cycle.[8] Nitric acid trihydrate (NAT) has received considerable attention as the most likely candidate for type I PSCs, due to its thermodynamic stability under polar stratospheric conditions. However, recent work suggests that nitric acid dihydrate (NAD) can also easily form and persist under similar conditions,[9−11] thus making NAD a potential component of type I PSCs.

Despite all of the attention PSCs have recently received, there remains much uncertainty concerning their actual composition. This is illustrated by a recent study of Toon and Tolbert[12] in which they were unable to simulate the aerosol spectra observed over Antarctica in 1987[13,14] with known frequency-dependent optical constants for several possible PSC components. The implication is that more laboratory work is needed to obtain refractive indices for candidate PSC species over a wide range of conditions, thus providing a more complete database for making such comparisons. In the case of NAD, for example, only two such studies have been reported: the first providing the real refractive index at 632 nm[15] and the second furnishing a set of frequency-dependent complex refractive indices between 480 and 7000 cm^{-1} at 184 K.[16]

In this paper we discuss the use of infrared aerosol extinction spectra to retrieve frequency-dependent complex refractive index data for NAD at 160, 180, and 190 K. We have demonstrated the usefulness of this approach previously for the case of water ice,[17] hydrazine,[18] and NAT[19] aerosols. The present optical constants are in reasonable agreement with those obtained from previous thin-film experiments;[16] however, there are several significant differences between the data sets, particularly below 1500 cm^{-1}. On the basis of a careful examination of several previously reported NAD aerosol[11,20] and thin-film spectra,[16,21,22] we conclude that the discrepancies between the refractive index sets are related to the manner in which NAD is produced in the two types of experiments. Comparisons between the various data sets suggest that the aerosol results are representative of unperturbed NAD. The NAD aerosol optical constants show a weak dependence on temperature over the range of this study, in contrast with the strong temperature dependence of water ice refractive indices.[17]

Experiment

The aerosols of interest were formed in a laminar aerosol flow cell described in detail elsewhere.[17,19,23] Briefly, the cell consists of a vertical tube with four independently controlled cooling regions. The temperature in each region is measured by a thermocouple to ±1 K. The cell configuration allows aerosols to be formed and observed at different temperatures. Independent control of the temperature in the formation region is important since the corresponding particle size distribution depends critically upon temperature, as well as cell pressure, vapor composition, and gas flow. In the present experiments, a saturated, room-temperature mixture of water and nitric acid vapor is entrained in a nitrogen buffer flow and injected into the top region of the cell. The vapor supersaturates upon entering the cell, as it is suddenly cooled to a temperature

between 160 and 170 K, causing particles to form via homogeneous nucleation and grow by condensation. The particles then flow into the other sections of the cell, which can be either warmer or colder than the formation region. The aerosol composition is varied by adjusting the composition of the vapor entering the cell using MKS mass flow controllers. We found that the purest NAD aerosols were obtained when the gas-phase water to nitric acid ratio was approximately 3:1, as determined by recording a high-resolution infrared spectrum of the gas mixture at room temperature with a Bomem DA3.02 Fourier transform infrared (FT-IR) spectrometer. All of the aerosol spectra reported here represent 100 coadditions recorded through the lowest view port of the flow cell. The FT-IR spectrometer was operated at a resolution of 2 cm^{-1} over the range from 700 to 4700 cm^{-1}. Typical spectra were recorded while the gas was flowing under laminar conditions, with mass flow rates ranging from 500 to 3000 standard cubic centimeters per minute (sccm) and at cell pressures between 50 and 700 Torr. Under these conditions, the aerosols have a typical residence time of 1 min in the flow cell. In a few experiments, however, the flow was stopped in order to observe the evolution of the spectra as a function of time.

Results and Discussion

Since the aerosol composition can be varied continuously over a wide range, the first step was to ensure that pure NAD could be produced and identified. A large number of experiments were thus carried out under a wide range of conditions, varying flow rates, vapor composition, cell pressure, and temperature in both the nucleation and observation regions. In general, we found that NAD was easier to form than NAT, which is consistent with observations by other workers[9−11] and is likely due to the fact that NAD has a slightly lower nucleation barrier than NAT, even though the latter is the most stable nitric acid hydrate under stratospheric conditions. A full discussion of our previous work on the NAT system is given elsewhere.[19]

The composition of the particles was controlled by varying the amount of water vapor injected into the cell. When the gas-phase water to nitric acid ratio was greater than 3:1, mixed NAD/NAT particles were formed, while vapor ratios less than this resulted in the formation of particles similar to those identified by other workers as amorphous nitric acid monohydrate (NAM).[22,24,25] To aid in the identification of a pure NAD spectrum, we conducted a few experiments under static conditions where the cell was charged with an aerosol and the flow suddenly stopped. As illustrated by the disappearance of NAT spectral features in Figure 1, we observed that the particles had a tendency to dehydrate as they aged. Since the water vapor pressure over the particles is greater than that of nitric acid, water vapor preferentially evaporates from the particles and condenses on the cell wall, thus effectively dehydrating the suspended aerosols.

Although the series of spectra in Figure 1 is a compilation of several different runs, qualitatively it can be viewed as a time-dependent series in a static cell going from pure NAT at the top to pure NAD at the bottom. There are several sharp features in the infrared spectrum of NAD and NAT that can be used to differentiate between them.[20,24,26] The distinctness of the features between 700 and 1100 cm^{-1} is further illustrated in the expanded view of the lower frequency region shown in Figure 2. For example, the peak at 1030 cm^{-1} is quite intense in the NAD spectrum and completely absent in the upper NAT spectrum. In addition, the sharp peak near 3500 cm^{-1} occurs
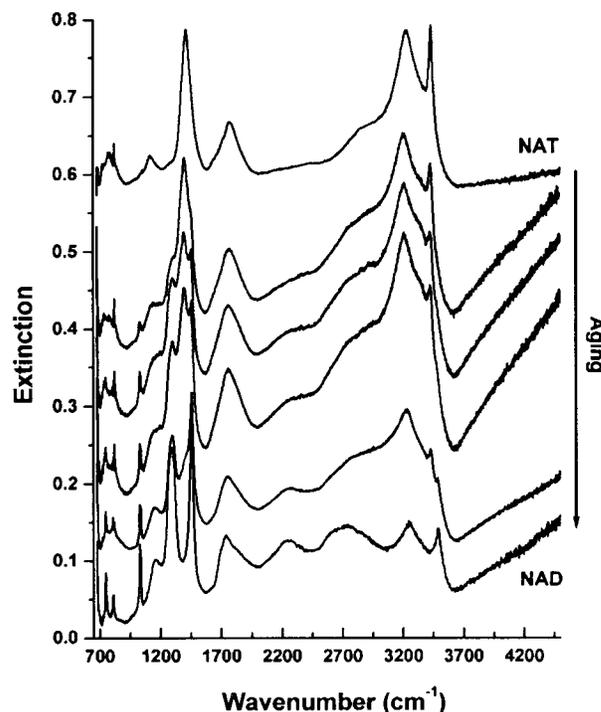
Figure 1. A series of spectra, recorded under static cell conditions, show the time evolution of nitric acid aerosol particles. The top and bottom spectra correspond to pure nitric acid trihydrate (NAT) and pure nitric acid dihydrate (NAD), respectively. The middle spectra correspond to mixed NAT/NAD aerosols and illustrate the transition that occurs as water is removed from the particles due to condensation on the cell walls.
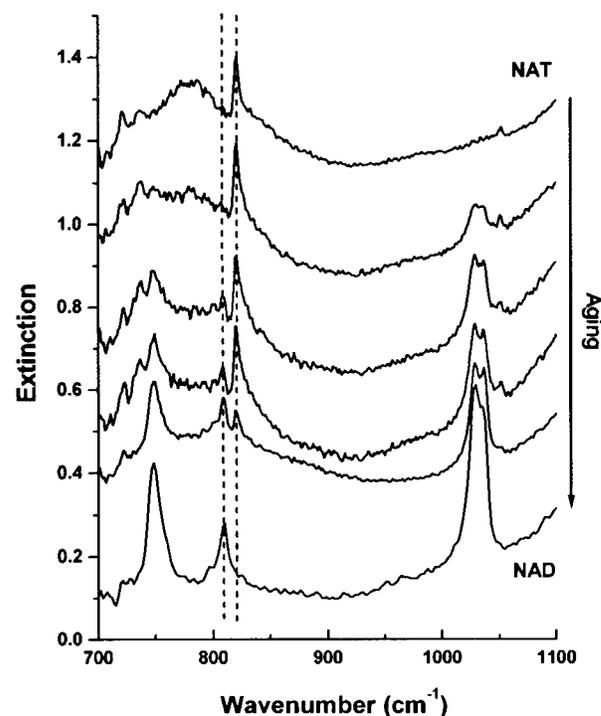
Figure 2. An expanded view of the lower frequency region of the spectra shown in Figure 1 showing several sharp bands, two of which are highlighted with vertical dashed lines, that can be used to uniquely identify NAD and NAT.

at a slightly different frequency for NAD and NAT. This is illustrated in the second spectrum from the bottom in Figure 1, where both peaks are present, indicative of a mixture of NAT and NAD. In what follows, we use these features to ensure

Optical Constants for Nitric Acid Dihydrate

J. Phys. Chem. A, Vol. 102, No. 32, 1998 **6479**
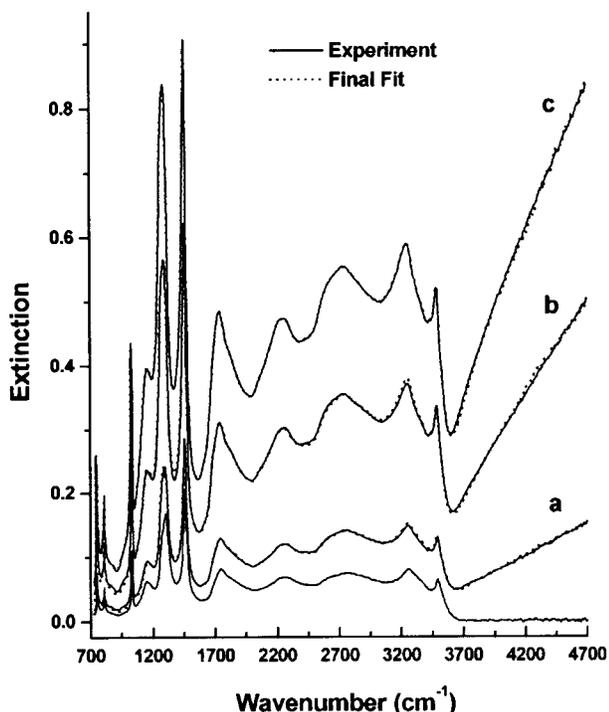
Figure 3. A series of NAD spectra at 180 K (solid lines) with corresponding Mie calculations (dotted line). The topmost spectrum was used in the fitting procedure while the nonscattering spectrum below was used for the determination of the initial complex refractive index data set. The fits to the two other spectra were obtained using the final index data set with only the particle size parameters (given) being varied. The log-normal size data for the top three spectra are as follows: (a) $r_{med} = 0.19$ μm, $\sigma = 0.53$; (b) $r_{med} = 0.33$ μm, $\sigma = 0.45$; (c) $r_{med} = 0.33$ μm, $\sigma = 0.50$.

that only pure NAD spectra were used to determine refractive indices.

NAD aerosol particles were studied over a wide range of particle sizes at three different temperatures, namely, 160, 180, and 190 K. In all, more than 50 spectra were recorded at each temperature, although not all were used in the present analysis. NAD particles were produced with median radii varying from 0.4 μm to slightly less than 0.1 μm, with a log-normal standard deviation of 0.5, as determined from Mie scattering simulations (discussed below). The purest NAD particles were formed when the nucleation region of the flow cell was held between 160 and 170 K. It was difficult to maintain pure NAD crystals outside of the observation range of 160−190 K. At higher temperatures, the particles tended to become mixtures of NAD and nonstoichiometric hydrates, while at lower temperatures NAT impurities were always present. Figure 3 shows several examples of NAD aerosol extinction spectra recorded at 180 K under different flow cell conditions. As expected, the scattering contribution becomes more important at the shorter wavelengths as the median particle size is increased. All of the aerosol spectra observed between 160 and 190 K are in good agreement with the NAD aerosol spectra recorded near 175 K by Bertram and Sloan[11] and Barton et al.[20]

NAD optical constants were determined from the aerosol extinction spectra using a method developed previously in our laboratory.[17−19] Briefly, a nonscattering aerosol spectrum recorded in the laboratory (e.g., the bottom spectrum in Figure 3) was used to estimate, within a scaling factor, the frequency-dependent imaginary component of the refractive index. Although this estimate is strictly only valid for bulk materials, it serves as a convenient approximation to initiate the retrieval

procedure. These scaled imaginary indices were used in a subtractive Kramers−Kronig transform[27] to calculate the corresponding real refractive indices. This routine requires a known value of the real refractive index at a frequency within the data set. We used the published real index value of 1.42 at 3980 cm^{-1} [16] in all of the present calculations.

It is well-known that the Kramers−Kronig transform is subject to truncation errors in the calculated real refractive indices, which manifest themselves as a rapid divergence in the real index at either end of the frequency range. To avoid this problem, we modified our procedure to artificially extend the imaginary refractive index set past our cell window cutoff at 700−400 cm^{-1}. A similar technique was employed by Toon et al.[16] in their thin-film optical constant work. We performed a spline interpolation of the Toon et al.[16] thin-film data between 480 and 700 cm^{-1}, which shows two weak bands, and spliced the results to our imaginary index set. A simple exponential function was used to finish the extension to 400 cm^{-1}. The inclusion of this extrapolated region in the Kramers−Kronig transform avoided the divergence problem in the real refractive index within the frequency range of the current study, namely, 700−4700 cm^{-1}.

The next step in the procedure involves selecting a large particle spectrum with a strong scattering component, such as the top spectrum in Figure 3. Such spectra are sensitive to both the real and imaginary components of the refractive index and thus provide us with spectral structure that can be used to determine the imaginary index scaling factor mentioned above. This is done by guessing a log-normal distribution of particle sizes[28] and calculating the spectrum with Mie scattering theory,[29] using the initial refractive index set determined above. The size distribution and imaginary index scaling factor are then varied until the residuals of the calculated and experimental spectra are minimized. This procedure is not unique unless the particle spectrum has a very strong scattering component. Other groups have noted the uniqueness problems that one can experience when fitting aerosol spectra using Mie theory,[10,11] and we were careful to avoid the conditions where these problems arose. Although Mie theory is only strictly valid for spherical particles, we and others[30,31] have found that, except under conditions where the refractive indices take on extremely large values, averaging over particle size removes much of the sensitivity to the particle shape. We previously confirmed this by carrying out discrete dipole calculations for other aerosol systems of various shapes and found that they agree very well with the results of Mie scattering theory after averaging over a log-normal size distribution.[32]

In following the above procedure, we found that some fitted band positions did not agree with the experimental results. These discrepancies arise from the fact that we initiated our fitting process using a nonscattering aerosol spectrum as a first guess of the imaginary refractive index. As mentioned above, this approximation is strictly valid only for bulk materials and does not account for the scattering of light by finite-sized particles. Following Bohren and Huffman,[29] we corrected the imaginary indices using the following expression:

$$k' = k\left(\frac{9n}{(n^2 + k^2 + 2)^2 + 4n^2k^2}\right)$$

where n and k are the first guess real and imaginary refractive indices, respectively. The new imaginary indices, k', were then used in place of the original data set, and the entire fitting process was repeated. This correction shifted all of the calculated peaks into agreement with the experimental results,
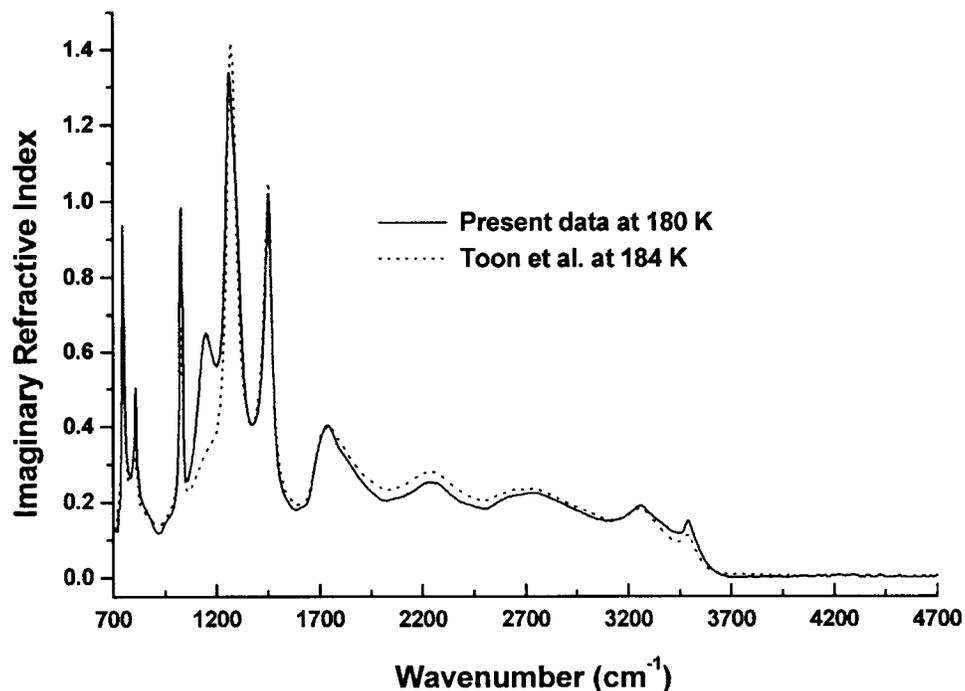
Figure 4. A comparison of the imaginary refractive index set for NAD at 180 K (solid line) with the thin-film data set for NAD at 184 K by Toon et al.[16] (dotted line). The major difference occurs near 1150 cm^{-1} where we observe a band (ν_2 hydronium ion bending mode) that is absent in the Toon et al. data.
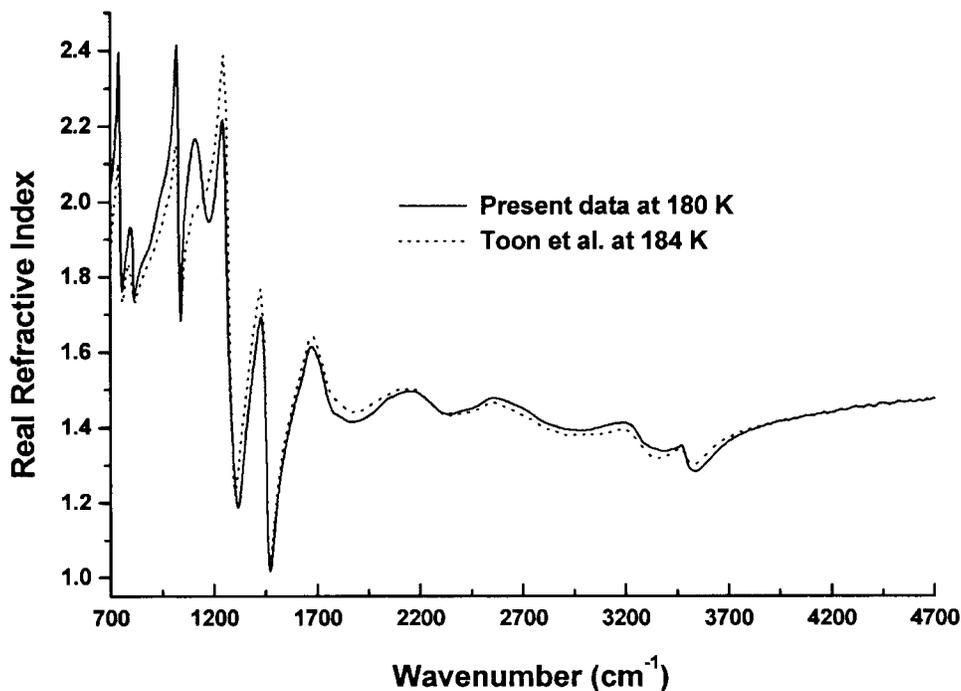
Figure 5. A comparison of the real refractive index set for NAD at 180 K (solid line) with the thin-film data set for NAD at 184 K by Toon et al.[16] (dotted line).

as shown in Figure 3. We applied the retrieval procedure to several scattering spectra to ensure convergence to a common set of refractive indices for each temperature. In general, the resulting scaling factors for the imaginary indices agreed to within 3%. The smallest value of the imaginary index that can be measured with our method is limited by the amount of noise in the extinction spectra at high wavenumber. We estimate the uncertainty in the imaginary index to be ±0.005 index units in this region of the spectrum.

The final refractive index data set used to generate the fits shown in Figure 3 is presented in Figures 4 and 5, along with the data set published previously from thin-film studies at 184 K by Toon et al.[16] The present data at 180 K are also summarized in Table 1 for a limited number of wavelengths. Overall, the agreement between the two data sets is quite reasonable. Nevertheless, careful inspection of the data reveals some significant differences in the intensity of the bands, particularly those below 1500 cm^{-1}. The most dramatic difference is in the band at 1150 cm^{-1} which is absent in the thin-film data set.[16] This band, which has been attributed to the ν_2 symmetric bending mode of the hydronium ion by Ritzhaupt and Devlin,[24] is quite prominent in the data set

TABLE 1: Refractive Indices for NAD at 180 K

cm^{-1}	k	n	cm^{-1}	k	n	cm^{-1}	k	n
4696.96	0.0054	1.477	3053.51	0.1540	1.398	1255.74	1.2637	2.050
4673.82	0.0031	1.473	3030.36	0.1587	1.395	1253.81	1.2177	2.098
4650.67	0.0004	1.471	3007.21	0.1633	1.393	1251.88	1.1659	2.138
4627.52	0.0029	1.473	2984.07	0.1686	1.393	1248.02	1.0545	2.191
4604.37	0.0004	1.469	2960.92	0.1758	1.393	1224.88	0.6394	2.132
4581.23	0.0002	1.471	2937.77	0.1809	1.394	1201.73	0.5605	2.000
4558.08	0.0003	1.467	2914.62	0.1867	1.396	1178.58	0.5934	1.947
4534.93	0.0020	1.469	2891.48	0.1936	1.398	1155.43	0.6459	1.992
4511.79	0.0038	1.465	2868.33	0.1995	1.402	1153.50	0.6484	2.001
4488.64	0.0033	1.462	2845.18	0.2045	1.406	1151.58	0.6504	2.011
4465.49	0.0012	1.463	2822.04	0.2103	1.410	1149.65	0.6510	2.020
4442.34	0.0034	1.464	2798.89	0.2163	1.416	1147.72	0.6507	2.031
4419.20	0.0063	1.458	2775.74	0.2217	1.423	1145.79	0.6497	2.041
4396.05	0.0014	1.457	2752.59	0.2246	1.432	1143.86	0.6478	2.053
4372.90	0.0043	1.458	2729.45	0.2249	1.441	1141.93	0.6446	2.064
4349.75	0.0009	1.453	2706.30	0.2229	1.448	1140.00	0.6391	2.075
4326.61	0.0013	1.455	2683.15	0.2208	1.454	1132.29	0.6077	2.116
4303.46	0.0067	1.454	2660.01	0.2187	1.460	1109.14	0.4602	2.167
4280.31	0.0064	1.448	2636.86	0.2167	1.465	1085.99	0.3284	2.110
4257.17	0.0045	1.446	2613.71	0.2137	1.470	1062.84	0.2629	1.994
4234.02	0.0064	1.446	2590.56	0.2076	1.475	1049.34	0.2634	1.856
4210.87	0.0060	1.440	2567.42	0.2008	1.478	1047.41	0.2707	1.822
4187.72	0.0043	1.438	2544.27	0.1917	1.477	1045.48	0.2859	1.782
4164.58	0.0023	1.440	2521.12	0.1842	1.471	1043.56	0.3184	1.736
4141.43	0.0027	1.436	2497.97	0.1819	1.463	1041.63	0.3830	1.695
4118.28	0.0049	1.433	2474.83	0.1851	1.456	1039.70	0.4968	1.684
4095.13	0.0022	1.432	2451.68	0.1884	1.450	1037.77	0.6443	1.725
4071.99	0.0033	1.431	2428.53	0.1933	1.447	1035.84	0.7366	1.778
4048.84	0.0034	1.427	2405.39	0.1968	1.444	1033.91	0.7531	1.815
4025.69	0.0023	1.423	2382.24	0.2018	1.440	1031.98	0.7972	1.870
4002.55	0.0030	1.421	2359.09	0.2102	1.437	1030.05	0.8935	1.960
3979.40	0.0000	1.420	2335.94	0.2196	1.436	1028.12	0.9829	2.093
3956.25	0.0009	1.418	2312.80	0.2314	1.438	1026.19	0.9765	2.230
3933.10	0.0029	1.414	2289.65	0.2436	1.445	1024.27	0.8549	2.332
3909.96	0.0034	1.410	2266.50	0.2503	1.458	1022.34	0.6951	2.392
3886.81	0.0013	1.408	2243.35	0.2520	1.468	1020.41	0.5585	2.414
3863.66	0.0018	1.403	2220.21	0.2515	1.479	1016.55	0.3911	2.391
3840.52	0.0018	1.398	2197.06	0.2456	1.490	1014.62	0.3437	2.366
3817.37	0.0011	1.395	2173.91	0.2370	1.495	1012.69	0.3087	2.341
3794.22	0.0022	1.391	2150.77	0.2286	1.496	1010.76	0.2830	2.317
3771.07	0.0014	1.384	2127.62	0.2222	1.494	1008.83	0.2630	2.295
3747.93	0.0010	1.378	2104.47	0.2156	1.491	1006.91	0.2465	2.274
3724.78	0.0001	1.372	2081.32	0.2111	1.485	993.40	0.1909	2.173
3701.63	0.0011	1.364	2058.18	0.2083	1.480	970.26	0.1608	2.079
3678.48	0.0030	1.353	2035.03	0.2050	1.473	947.11	0.1404	2.026
3655.34	0.0052	1.343	2011.88	0.2048	1.460	923.96	0.1192	1.967
3632.19	0.0120	1.330	1988.73	0.2104	1.447	900.81	0.1276	1.905
3609.04	0.0214	1.317	1965.59	0.2205	1.437	877.67	0.1598	1.866
3585.90	0.0347	1.303	1942.44	0.2315	1.429	854.52	0.1837	1.838
3562.75	0.0549	1.290	1919.29	0.2450	1.422	831.37	0.2204	1.792
3539.60	0.0830	1.284	1896.15	0.2606	1.417	821.73	0.2707	1.766
3516.45	0.1148	1.289	1873.00	0.2782	1.415	819.80	0.2861	1.767
3502.95	0.1375	1.301	1849.85	0.2982	1.417	817.87	0.2919	1.761
3501.02	0.1406	1.304	1826.70	0.3170	1.424	815.94	0.2993	1.750
3499.09	0.1430	1.308	1803.56	0.3341	1.432	814.01	0.3274	1.741
3497.16	0.1454	1.312	1780.41	0.3574	1.439	812.08	0.3884	1.751
3495.24	0.1475	1.316	1757.26	0.3889	1.467	810.15	0.4738	1.805
3493.31	0.1488	1.320	1734.12	0.4033	1.519	808.22	0.5032	1.863
3491.38	0.1494	1.324	1710.97	0.3782	1.572	806.30	0.4456	1.894
3489.45	0.1494	1.329	1687.82	0.3307	1.605	804.37	0.3870	1.915
3487.52	0.1487	1.333	1664.67	0.2598	1.612	802.44	0.3596	1.926
3485.59	0.1474	1.337	1641.53	0.2024	1.565	800.51	0.3452	1.930
3483.66	0.1456	1.340	1618.38	0.1883	1.513	798.58	0.3330	1.931
3481.73	0.1434	1.344	1595.23	0.1812	1.468	796.65	0.3224	1.934
3479.80	0.1407	1.346	1572.08	0.1825	1.414	794.72	0.3089	1.932
3470.16	0.1258	1.352	1548.94	0.1979	1.355	785.08	0.2652	1.899
3466.30	0.1214	1.351	1525.79	0.2230	1.286	771.58	0.2882	1.837
3464.37	0.1198	1.351	1502.64	0.2780	1.183	769.65	0.2966	1.826
3462.44	0.1188	1.350	1479.50	0.4624	1.041	767.72	0.3070	1.815
3460.51	0.1182	1.349	1456.35	0.9824	1.213	765.79	0.3214	1.803
3458.59	0.1179	1.348	1454.42	1.0106	1.276	763.86	0.3406	1.792

TABLE 1 (Continued)

cm^{-1}	k	n	cm^{-1}	k	n	cm^{-1}	k	n
3456.66	0.1176	1.348	1452.49	1.0201	1.340	761.93	0.3642	1.781
3454.73	0.1174	1.347	1450.56	1.0118	1.401	760.00	0.3937	1.771
3447.01	0.1174	1.345	1448.63	0.9915	1.457	758.07	0.4311	1.763
3423.86	0.1200	1.342	1446.70	0.9643	1.506	756.14	0.4802	1.761
3400.72	0.1267	1.338	1433.20	0.7264	1.683	754.21	0.5433	1.767
3377.57	0.1369	1.338	1410.05	0.4840	1.642	752.29	0.6244	1.791
3354.42	0.1474	1.342	1386.91	0.4135	1.540	750.36	0.7242	1.842
3331.28	0.1570	1.345	1363.76	0.4111	1.431	748.43	0.8386	1.942
3308.13	0.1685	1.352	1340.61	0.4773	1.298	746.50	0.9365	2.102
3284.98	0.1807	1.360	1317.46	0.7116	1.188	744.57	0.9097	2.262
3261.83	0.1900	1.380	1294.32	1.0429	1.312	742.64	0.7243	2.359
3238.69	0.1849	1.400	1271.17	1.2728	1.628	740.71	0.5048	2.395
3215.54	0.1743	1.409	1269.24	1.2925	1.668	738.78	0.3482	2.386
3192.39	0.1642	1.413	1267.31	1.3095	1.712	736.85	0.2638	2.353
3169.24	0.1574	1.412	1265.38	1.3237	1.760	734.93	0.2205	2.312
3146.10	0.1530	1.411	1263.45	1.3361	1.816	733.00	0.1974	2.274
3122.95	0.1506	1.407	1261.53	1.3383	1.876	731.07	0.1843	2.241
3099.80	0.1511	1.405	1259.60	1.3264	1.937	729.14	0.1798	2.218
3076.66	0.1524	1.401	1257.67	1.3010	1.996	715.64	0.1244	2.108

obtained here and has been observed in other infrared spectra of NAD aerosols.[11,20]

In view of the significant differences between the present results and those of the previous thin-film study, it is obviously important that we consider both the source of these differences and the question of which data set is more appropriate for use in PSC modeling. As noted previously, we have studied NAD aerosols under a variety of conditions and have never observed differences as large as those between the aerosol and thin-film results. In addition, the present infrared spectra are in excellent agreement with previous aerosol studies, as shown in Figure 6, indicating that the problem is not associated with the way the measurements are being done. In previous thin-film studies, however, the band intensities associated with the hydronium ion tend to be quite variable. Comparing the results of Toon et al.[16] with those obtained previously by other workers[22,24,25] reveals slight differences in the relative hydronium band intensities, even for the same substrate. Even more dramatic is the comparison with a recent study by Koch et al.[21] for a thin-film NAD sample on a gold substrate, obtained using reflection−absorption infrared spectroscopy. In this work, both the ν_2 hydronium ion band and the ν_2 nitrate (out-of-plane bending mode near 820 cm^{-1}) band were significantly enhanced relative to those in the Toon et al.[16] data set, as shown in Figure 6. Koch and co-workers attributed these observations to the orientation of the nitrate ions by the gold substrate.

The sensitivity of the NAD thin-film spectra to the nature of the substrate and/or the orientation of the crystal puts their usefulness in the modeling of PSCs in question and suggests that the optical constants obtained here from unsupported aerosols might be more reliable. While the assumptions made in our aerosol approach (concerning the effects of particle shape, for example) cannot be definitively validated, the overall self-consistency of the fitted parameters over a range of scattering effects is excellent. It is interesting to point out that Toon and co-workers (Toon, O. B., private communication, 1998) prefer to explain the differences between the various spectra as resulting from the growth of different phases of NAD. Although we cannot rule out this possibility, without any further evidence for the existence of these multiple phases, we are more inclined to explain the differences in terms of substrate interference. Indeed, there are many things that can lead to changes in vibrational band intensities. These two points of view are, in fact, only semantically different given that what we are saying is that the substrate changes the properties of the NAD that is
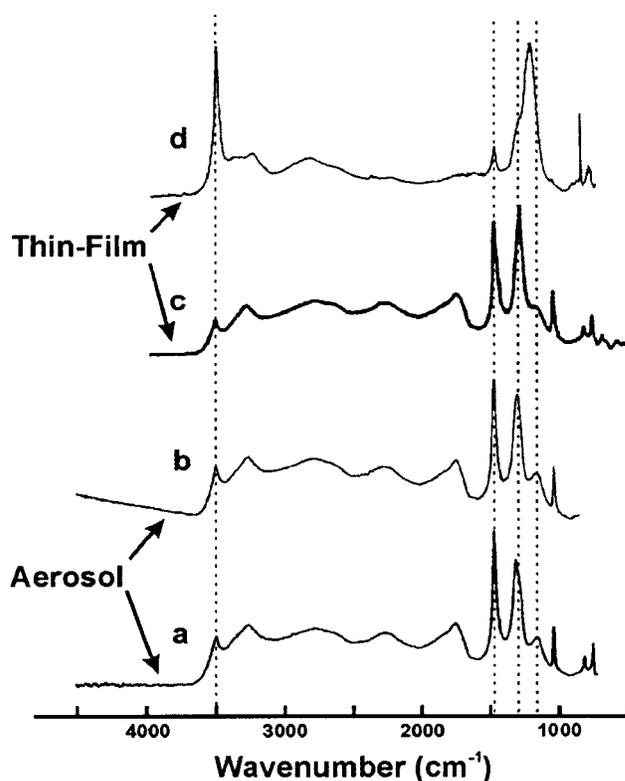
Figure 6. A comparison of four NAD spectra which demonstrates how spectral features can vary in thin-film studies. Spectra a (present study) and b (Bertram and Sloan[11]) are aerosol results. Spectra c (Tolbert et al.[22]) and d (Koch et al.[21]) are thin-film results. The thin-film results are quite different from each other and the aerosol results. The aerosol results, on the other hand, are self-consistent with each other.

produced. One could obviously call this a new phase, although we prefer to call it substrate perturbed NAD. Clearly, this study shows the importance of having alternative approaches for determining optical constants that can at the very least help assess the confidence with which these values are determined. Once again, the ability to determine such properties from unsupported samples is clearly a step forward.

The temperature dependence of the NAD optical constants was found to be rather weak over the temperature range studied here as illustrated by the expanded views of the refractive index data sets in Figure 7. Indeed, the imaginary refractive indices decrease barely (5%) in the nitrate stretch region (Figure 7a)
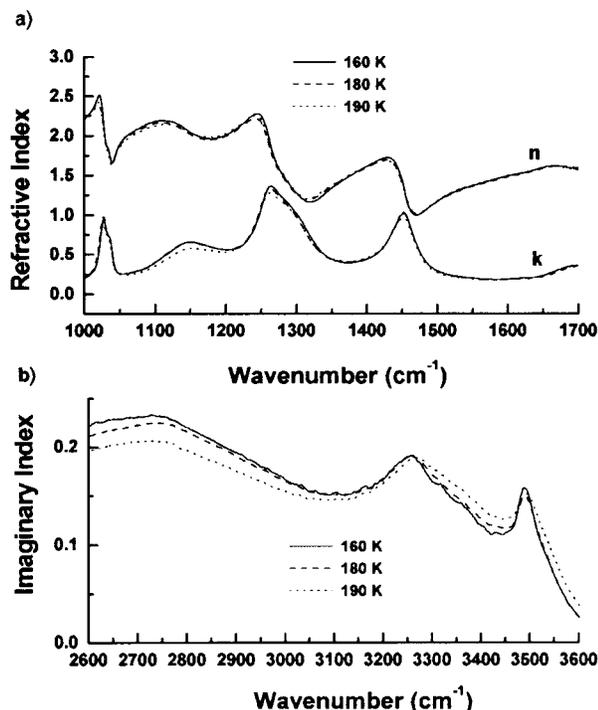
Figure 7. (a) An expanded view of the NAD refractive indices at 160 K (solid line), 180 K (dashed line), and 190 K (dotted line) in the nitrate stretching region centered around 1350 cm^{-1}. (b) An expanded view of the NAD imaginary indices in the O–H stretching region near 3 μm at 160 K (solid line), 180 K (dashed line), and 190 K (dotted line).

below 1500 cm^{-1} with increasing temperature. The imaginary indices in the O–H stretch region near 3 μm (Figure 7b) decrease (and broaden) slightly as the temperature is increased. These results are in stark contrast to the previously observed temperature dependence of water ice optical constants, where the 3 μm band shifts to higher frequency and broadens substantially with increasing temperature.[17]

Understanding the difference between these two systems requires some discussion of the water ice spectrum, which has been studied extensively.[33–39] Of particular interest in this case is the strong intermolecular coupling between the individual O–H oscillators. The work of Sivakumar et al.[40] on the infrared and Raman spectra of polycrystalline ice and amorphous solid water indicates that the blue shift of the 3 μm band with increasing temperature is simply related to changes in the average distance between oxygen sites in the ice lattice caused by the thermal expansion of the crystal. On the other hand, the much stronger temperature dependence of the 3 μm band shape could not be accounted for in this way and was instead attributed to rather strong coupling between high-frequency O–H oscillators and low-frequency vibrational modes of the crystal lattice.[41] As a result, the O–H band should not be viewed as an assembly of individual local oscillators, but rather a more delocalized, coupled set of oscillators. A great deal of work on dilute isotopic mixtures has indeed shown that isolated O–H oscillators give a much different (narrower) spectrum than observed for normal water ice.

Given these considerations, we conclude that the weak temperature dependence observed for the NAD optical constants results from much weaker intermolecular coupling. This is consistent with the fact that the O–H stretching region of NAD is considerably narrowed, showing more structure than observed for pure water ice. In addition, the ionic character of NAD crystals makes a more rigid structure, compared with the pure

hydrogen-bonded network found in water ice, making the corresponding structure less sensitive to changes in temperature. Further insights into this phenomena might be forthcoming if the crystal structure of NAD were known. Unfortunately, no such structural determination has been reported in the literature for NAD.[42]

The optical constant data sets for NAD all three temperatures are available from the authors upon request. Alternatively, the refractive indices are stored in ASCII files and can be downloaded from our anonymous FTP site, ftp://frenchie.chem.unc.edu.

Summary

We report here the first direct determination of the frequency-dependent optical constants for NAD from aerosol extinction spectra at several temperatures between 160 and 190 K. The aerosol spectra used to retrieve the refractive indices are in excellent agreement with other NAD aerosol studies.[11,20] Nevertheless, there are some significant differences between the current indices and those obtained previously in thin-film studies.[16] Comparisons with other thin-film data suggest that these differences are indicative of substrate perturbations of NAD. We maintain that the aerosol data presented here provide a measure of the optical constants of unperturbed NAD. Although the differences remain to be definitively explained and the results tested in various applications, the present results clearly show that direct measurements on aerosols are extremely important in assessing the level of confidence that can be placed in thin-film measurements. We also find that the optical constants of NAD show only a weak dependence on temperature over the range studied here. This is in contrast to our previous results for water ice[17] and suggests that intermolecular coupling within the NAD crystal is rather weak.

References and Notes

(1) Solomon, S. *Rev. Geophys.* **1988,** *26,* 131.
(2) Crutzen, P. J.; Arnold, F. *Nature* **1986,** *324,* 651.
(3) Poole, L. R.; McCormick, M. P. *J. Geophys. Res.* **1988,** *93,* 8423.
(4) Hofmann, D. J.; Deshler, T. L.; Aimedieu, P.; et al. *Nature* **1989,** *340,* 117.
(5) Hamill, P.; Toon, O. B. *Phys. Today* **1991,** *44,* 34.
(6) Toon, O. B.; Hamill, P.; Turco, R. P.; Pinto, J. *Geophys. Res. Lett.* **1986,** *13,* 1284.
(7) Salawitch, R. J.; Gobbi, G. P.; Wofsy, S. C.; McElroy, M. B. *Nature* **1989,** *339,* 525.
(8) Mulvaney, R.; Wolff, E. W. *J. Geophys. Res.* **1993,** *98,* 5213.
(9) Worsnop, D. R.; Fox, L. E.; Zahniser, M. S.; Wofsy, S. C. *Science* **1993,** *259,* 71.
(10) Disselkamp, R. S.; Anthony, S. E.; Prenni, A. J.; Onsach, T. B.; Tolbert, M. A. *J. Phys. Chem.* **1996,** *100,* 9127.
(11) Bertram, A. K.; Sloan, J. J. *J. Geophys. Res.* **1998,** *103,* 3553.
(12) Toon, O. B.; Tolbert, M. A. *Nature* **1995,** *375,* 218.
(13) Kinne, S.; Toon, O. B.; Toon, G. C.; Farmer, C. B.; Browell, E. V.; McCormick, M. P. *J. Geophys. Res.* **1989,** *94,* 16481.
(14) Toon, G. C.; Farmer, C. B.; Lowes, L. L.; Schaper, P. W.; Blavier, J.-F.; Norton, R. H. *J. Geophys. Res.* **1989,** *94,* 16571.
(15) Berland, B. S.; Haynes, D. R.; Foster, K. L.; Tolbert, M. A.; George, S. M.; Toon, O. B. *J. Phys. Chem.* **1994,** *98,* 4358.
(16) Toon, O. B.; Tolbert, M. A.; Koehler, B. G.; Middlebrook, A. M.; Jordan, J. *J. Geophys. Res.* **1994,** *99,* 25631.
(17) Clapp, M. L.; Worsnop, D. R.; Miller, R. E. *J. Phys. Chem.* **1995,** *99,* 6317.
(18) Clapp, M. L.; Miller, R. E. *Icarus* **1996,** *123,* 396.

(19) Richwine, L. J.; Clapp, M. L.; Miller, R. E.; Worsnop, D. R. *Geophys. Res. Lett.* **1995,** *22,* 2625.

(20) Barton, N.; Rowland, B.; Devlin, J. P. *J. Phys. Chem.* **1993,** *97,* 5848.

(21) Koch, T. G.; Holmes, N. S.; Roddis, T. B.; Sodeau, J. R. *J. Phys. Chem.* **1996,** *100,* 11402.

(22) Tolbert, M. A.; Koehler, B. G.; Middlebrook, A. M. *Spectrochim. Acta* **1992,** *48,* 1363.

(23) Clapp, M. L.; Niedziela, R. F.; Richwine, L. J.; Dransfield, T.; Miller, R. E.; Worsnop, D. R. *J. Geophys. Res.* **1997,** *102,* 8899.

(24) Ritzhaupt, G.; Devlin, J. P. *J. Phys. Chem.* **1991,** *95,* 90.

(25) Koehler, B. G.; Middlebrook, A. M.; Tolbert, M. A. *J. Geophys. Res.* **1992,** *97,* 8065.

(26) Tolbert, M. A.; Middlebrook, A. M. *J. Geophys. Res.* **1990,** *95,* 22423.

(27) Palmer, K. F.; Wood, B. E.; Roux, J. A. AEDC-TR-80-30*,* 1981 (AD-AO94214).

(28) Kerker M. *The Scattering of Light and Other Electromagnetic Radiation;* Academic Press: New York, 1969.

(29) Bohren, C. F.; Huffman, D. R. *Absorption and Scattering of Light by Small Particles;* Wiley: New York, 1983.

(30) Holland, A. C.; Draper, J. S. *Appl. Opt.* **1967,** *6,* 511.

(31) Perry, R. J.; Hunt, A. J.; Huffman, D. R. *Appl. Opt.* **1978,** *17,* 2700.

(32) Clapp, M. L.; Miller, R. E. *Icarus* **1993,** *105,* 529.

(33) Bertie, J. E.; Whalley, E. *J. Chem. Phys.* **1964,** *40,* 1637.

(34) Whalley, E. *Can. J. Chem.* **1977,** *55,* 3429.

(35) McGraw, R.; Madden, W. G.; Bergren, M. S.; Rice, S. A.; Sceats, M. G. *J. Chem. Phys.* **1978,** *69,* 3483.

(36) Madden, W. G.; Bergren, M. S.; McGraw, R.; Rice, S. A.; Sceats, M. G. *J. Chem. Phys.* **1978,** *69,* 3497.

(37) Bergren, M. S.; Schuh, D.; Sceats, M. G.; Rice, S. A. *J. Chem. Phys.* **1978,** *69,* 3477.

(38) Bergren, M. S.; Rice, S. A. *J. Chem. Phys.* **1982,** *77,* 583.

(39) Rice, S. A.; Bergren, M. S.; Belch, A. C.; Nielson, G. *J. Phys. Chem.* **1983,** *87,* 4295.

(40) Sivakumar, T. C.; Schuh, D.; Sceats, M. G.; Rice, S. A. *Chem. Phys. Lett.* **1977,** *48,* 212.

(41) Sivakumar, T. C.; Rice, S. A.; Sceats, M. G. *J. Chem. Phys.* **1978,** *69,* 3468.

(42) Koch, T. G.; Holmes, N. S.; Roddis, T. B.; Sodeau, J. R. *J. Chem. Soc., Faraday Trans.* **1996,** *92,* 4787.